ORGANIC
CHEMISTRY
FRONTIERS

Check for updates

Asymmetric living supramolecular polymerization of an achiral aza-BODIPY dye by solvent-mediated chirality induction and memory†

Jiahui Ding, [ID] Hongfei Pan, Houchen Wang, Xiang-Kui Ren [ID] and Zhijian Chen [ID] *

The kinetic self-assembly properties of an achiral aza-BODIPY dye **1** bearing two hydrophobic fan-shaped tridodecyloxybenzamide pendants through 1,2,3-triazole linkages were investigated in detail in chiral solvents (S)- and (R)-limonene by UV/Vis absorption spectroscopy, CD spectroscopy, AFM, and TEM. The spectroscopic studies indicated the formation of thermodynamic H-aggregates (**Agg. II$_L$**) with a helical morphology, while metastable aggregates (**Agg. I$_L$**) could only be observed in the fast cooling process of **1** in limonene. According to further analysis of the spectroscopic data using the nucleation–elongation model, the mechanistic aspects of the self-assembly process of dye **1** were elucidated. The macroscopic chirality and helicity of supramolecular aggregates were found to be dependent on the chirality of the limonene solvents. Since the kinetic trapping of **Agg. I$_L$** could not be attained in experiments, an effective strategy for asymmetrical living supramolecular polymerization (LSP) of dye **1** was developed by employing the seeds in the chiral solvent limonene and the kinetically-trapped metastable aggregates (**Agg. I$_M$**) in methylcyclohexane (MCH). The chiral aggregates **Agg. II$_L$** were obtained by multiple-cyclic LSP in the MCH/limonene solvent mixture even at a very low limonene ratio (less than 1%), which could be ascribed to the chiral memory effect of dye **1** aggregates upon continuous dilution of the chiral environment in the solvent mixture during the LSP process.
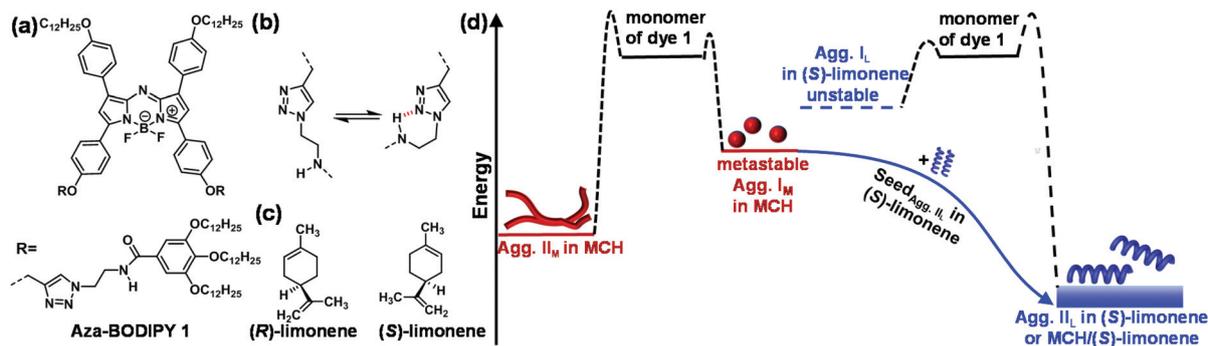
Introduction

In the recent decade, molecular aggregates with supramolecular chirality[1] have gained considerable attention and been investigated widely due to their assembly mechanism[2] and applications, such as in chiral recognition and sensing,[3] supramolecular chiral catalysis,[4] chiral optic and electronic devices,[5] and biomaterials.[6] It has been demonstrated that for π-conjugated molecules, such as porphyrins,[7] oligo(*p*-phenylene vinylene)s,[8] perylene and naphthalene bisimides,[9] hexabenzocoronenes,[10] *etc*., supramolecular chirality and structural helicity can be obtained for one-dimensional π-stacks by introducing side chains with a permanent chiral center. On the other hand, it is more challenging to construct chiral supramolecular assemblies from achiral building blocks since the resultant products are usually a mixture containing equal amounts of both right- and left-handed helical stacks and thus

racemic on the whole.[11] To introduce macroscopic supramolecular chirality as well as helicity bias in such systems, the employment of experimental conditions including chiral organic solvents,[12] chiral additives,[13] vortex motion by stirring,[14] and circular polarization light[15] has been reported. Furthermore, it has been found that the supramolecular chirality of assemblies can be first induced using small molecular chiral additives or chiral solvents and then maintained upon subsequent removal of the chiral inducers until the lowest thermodynamic state is reached. Such a chiral memory effect has been utilized as an important strategy for chirality imprinting in supramolecular assemblies composed of achiral building blocks.[16] Examples of the chiral memory effect using H-bonded acid additives,[17] as well as solvents[18] as chiral templates have been reported for the control of the handedness of supramolecular chirality of self-assembly systems.

In our previous work,[19] we reported the aza-BODIPY dye **1** (Scheme 1a) bearing two fan-shaped tridodecyloxybenzamide pendants, which exhibited biphasic assembly pathways towards kinetic-controlled metastable aggregates (**Agg. I$_M$**) and thermodynamic products (**Agg. II$_M$**) as well as the capability of living supramolecular polymerization (LSP) in the apolar solvent methylcyclohexane (MCH). The pathway complexity of dye **1** could be ascribed to the interconvertible intermolecular-

School of Chemical Engineering and Technology, The National Collaborative Innovation Center of Chemical Science and Engineering (Tianjin), Tianjin University, Tianjin, 300072, China. E-mail: zjchen@tju.edu.cn

This journal is © the Partner Organisations 2022

Org. Chem. Front., 2022, **9**, 3949–3955 | **3949**

Scheme 1 (a) Chemical structure of aza-BODIPY dye **1**. (b) Conformational interconversion of the intermolecular and intramolecular H-bond moieties in dye **1**. (c) Chemical structures of (S)- and (R)-limonene solvents. (d) Schematic illustration of the kinetic aggregation pathways of dye **1** in MCH (left) and (S)-limonene (right) for the unstable **Agg. I_L** and thermodynamically stable in chiral solvents and the metastable **Agg. I_M** in MCH can be transformed into the chiral **Agg. II_L** via seeded living supramolecular polymerization by adding the seed of **Agg. II_L** in (S)-limonene.

intramolecular H-bonding patterns (Scheme 1b) and π–π stacking interactions of the tetraphenyl-substituted aza-BF$_2$-dipyrromethene chromophores. In the current work, we further explored the supramolecular assembly of dye **1** in chiral nonpolar solvents, *i.e.* (S)- and (R)-limonene, and elaborated the impact of chiral bias imposed by the chiral solvents on the supramolecular chirality of the aggregates of achiral dye **1**.

Moreover, a strategy to control the supramolecular chirality of the dye **1** aggregates by asymmetrical LSP was proposed and investigated (Scheme 1d), in which the seeds of thermodynamic aggregates in the chiral solvent limonene (**Agg. II_L**) and the kinetically-trapped metastable aggregates in MCH (**Agg. I_M**) were used to obtain the chiral aggregates of dye **1** by exploiting the chiral memory effect of dye **1** aggregates upon continuous dilution of the chiral component in the MCH/limonene mixture during the multiple-cyclic LSP operation.

Results and discussion

In both (S)- and (R)-limonene, the self-assembly pathways of aza-BODIPY dye **1** were investigated by temperature- and concentration-dependent UV/Vis and CD spectroscopy. At 343 K, the characteristic absorption band for monomeric dye **1** was observed in (S)-limonene with an absorption maximum at 684 nm. When this solution was cooled quickly at a rate of 10 K min^{-1}, obvious spectral changes were observed (Fig. 1a). From 343 K to 317 K, the absorption band around 680 nm was gradually lowered with a slight bathochromic shift of the absorption maximum to 692 nm. Meanwhile, an increase in the absorption around 750 nm was also observed. Upon continuously decreasing the temperature from 317 K to 273 K, the absorption at 750 nm started to decrease while a new absorption band appeared at 595 nm with a large hypsochromic shift of *ca.* 90 nm with respect to the monomer band. The unusual spectral changes at 750 nm (Fig. 1a, inset) are comparable to those observed for dye **1** aggregation in MCH[19] and can be explained by the first formation of metastable aggregates (**Agg. I_L** in Scheme 1d), which quickly transformed into thermo-

dynamically more stable H-aggregates (**Agg. II_L**) upon further cooling. However, unlike **Agg. I_M** in MCH, it was observed that **Agg. I_L** in limonene could not be trapped kinetically even with a fast cooling rate of 20 K min^{-1}. Obviously, this character is disadvantageous for the use of **Agg. I_L** in further LSP studies. In contrast, upon slow cooling the monomer solution from 343 K to 273 K at a rate of 0.5 K min^{-1} (Fig. S1†), the spectral changes around 750 nm could not be detected anymore, while at the same cooling rate in MCH the appearance of metastable **Agg. I_M** could still be distinguished from the UV-Vis absorption spectra, implying that **Agg. I_L** in limonene is less stable than **Agg. I_M** in MCH. Similar kinetic aggregation behaviour was observed for dye **1** in (R)-limonene (Fig. S2†).

Furthermore, the chirality induction by the chiral solvent (S)-limonene towards the aggregates of dye **1** was investigated by CD spectroscopy (Fig. 1b). With a cooling rate of 0.5 K min^{-1} of dye **1** in (S)-limonene, a bisignated CD signal located at 582 nm started to rise from 315 K and reached the maximum at 273 K. This result is indicative of the formation of chiral supramolecular aggregates (**Agg. II_L**) of dye **1** in the homochiral limonene solvent. In addition, the sign of the observed CD signal of **Agg. II_L** depended on the chirality of the solvents, *i.e.* a negative Cotton effect was observed in (S)-limonene, while the Cotton effect in (R)-limonene was positive (Fig. S3†), suggesting that the helical sense of the π-stacks of aza-BODIPY **1** in (S)-limonene and (R)-limonene was opposite (Fig. S4†). According to the exciton chirality method,[18] the negative Cotton effect observed in (S)-limonene indicated the preferential formation of left-handed (M-configured) π-stacks of dye **1**, while right-handed (P-configured) helical stacks were more preferred in (R)-limonene.

For further mechanistic understanding of the aggregation process of dye **1** in chiral limonene, the nucleation–elongation model developed by van der Schoot *et al.*[20] was applied to analyse the temperature-dependent UV/Vis and CD spectroscopic data for dye **1**. The experimental and model-simulated fraction of aggregated molecules (α_{agg}) was plotted *vs.* temperature (Fig. 1c) and the resultant thermodynamic parameters, such as elongation temperature T_e and elongation enthalpies,
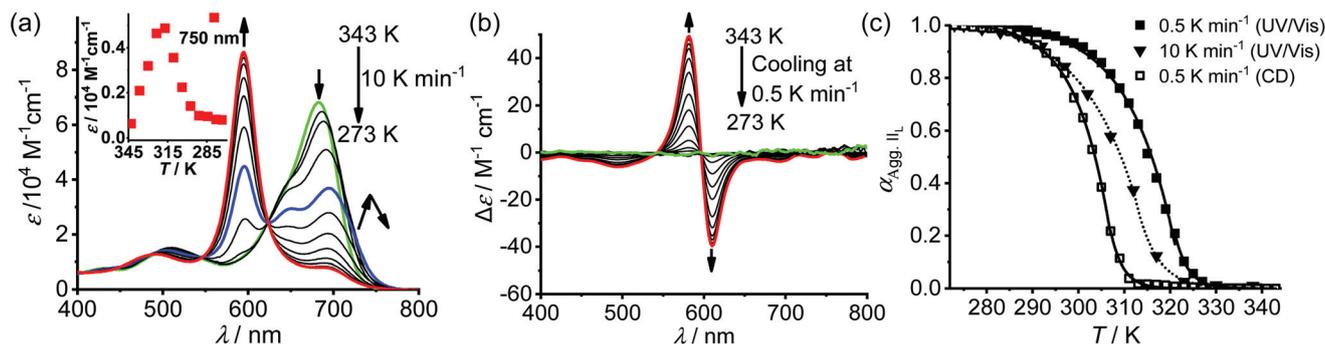
Fig. 1 (a) Temperature-dependent UV/Vis absorption spectra of dye **1** upon cooling from 343 K to 273 K at 10 K min^{-1} in (S)-limonene (1.0 × 10^{-5} M). Inset: changes of the molar absorption coefficient monitored at 750 nm. (b) Temperature-dependent CD spectra of dye **1** upon cooling from 343 K to 273 K in (S)-limonene (1.0 × 10^{-5} M) at 0.5 K min^{-1}. (c) The plot of the molar fraction of aggregates in the cooling process monitored using UV/Vis absorption (monitored at 595 nm) and CD spectra (monitored at 582 nm) versus temperatures at different cooling rates and fitted with the nucleation–elongation model, respectively.

are listed in Table 1. Accordingly, obvious thermal hysteresis of ca. 6 K was observed between the curves based on UV/Vis spectroscopy with a fast (10 K min^{-1}) and slow cooling rate (0.5 K min^{-1}), reflecting the kinetic assembly process of dye **1** and the formation of the metastable **Agg. I$_L$**. Moreover, the CD-based cooling curve at 0.5 K min^{-1} displayed a large thermal hysteresis of 13 K as compared with that based on UV/Vis spectroscopy. At T = 312 K, α_{agg} = 0.02 was given by the CD-based curve while an aggregate state with α_{agg} = 0.7 was indicated by the curve based on UV/Vis spectroscopy. Such thermal hysteresis as well as the thermodynamic parameters e.g. K_a and N_n obtained by CD and UV/Vis spectroscopy implied that several steps and intermediate aggregate species could be involved in the assembly process as observed for a H-bonded dimeric OPV system with chiral side chains by Meijer and co-workers[21] where UV/Vis absorption and CD spectroscopic data need to be considered in combination to give a whole mechanistic picture for the transition from the monomer to chiral aggregates (vide infra).

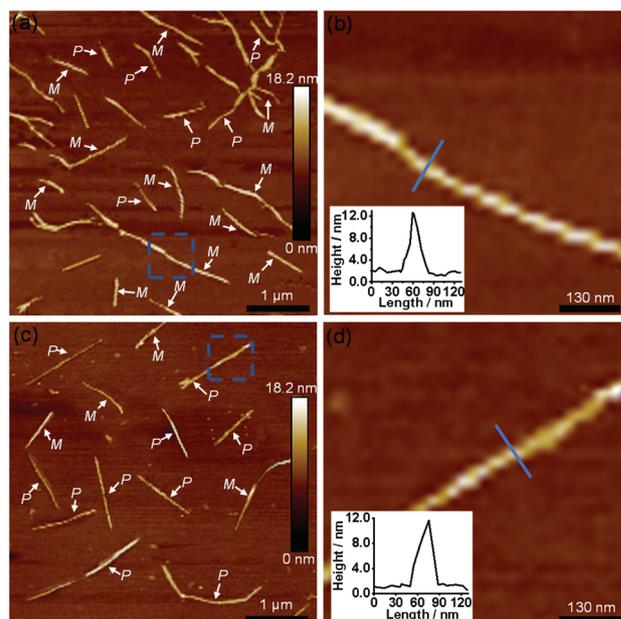In addition, the enthalpy and entropy contributions for the aggregation of dye **1** in (S)- and (R)-limonene were evaluated using the temperature-dependent spectroscopic data of heating processes (Fig. S5†) according to the equation $RT_e\ln(1/c_T) = \Delta H° - T_e\Delta S°$. From experiments at different total concentrations of dye **1** (5.0 × 10^{-6} M to 5.0 × 10^{-5} M), a van't Hoff plot of $\ln(1/c_T)$ versus T_e^{-1} showed a compliance with a linear relationship (Fig. S6†). The values of $\Delta H°$ and $\Delta S°$ for (S)-limonene were calculated to be −176 ± 3.2 kJ mol^{-1} and −352 ± 2.7 J mol^{-1} K^{-1}, respectively. In comparison with a $\Delta H°$ of −154 kJ mol^{-1} and a $\Delta S°$ of −349 J mol^{-1} K^{-1} in MCH,[19] the

supramolecular aggregates formed of dye **1** in (S)-limonene exhibited higher thermodynamic stability. On the other hand, the thermodynamic parameters obtained in (R)-limonene (Fig. S7 and Table S1†) were very close to those obtained in (S)-limonene. Within the error of the experiments, the data for these two solvents can be considered as identical.

The supramolecular chirality of dye **1** aggregates in limonene was further investigated by morphological studies of the nanoaggregates. For samples spin-cast from dye **1** solution in (S)- and (R)-limonene, fibrous helical aggregates of aza-BODIPY **1** were observed (Fig. 2a–d). These helical nanofibers

Fig. 2 (a) AFM height image of **Agg. II$_L$** by drop-casting the (S)-limonene solution (1.0 × 10^{-5} M) on mica. (b) Zoomed image of one left-handed (M) nanofiber in the area marked by a blue square in (a). Inset: cross-section analysis along the blue line. (c) AFM image of **Agg. II$_L$** by drop-casting the (R)-limonene solution (1.0 × 10^{-5} M) on mica. (d) Zoomed image of one right-handed (P) nanofiber in the area marked by a blue square in (c). Inset: cross-section analysis along the blue line.

Table 1 Thermodynamic parameters based on the nucleation–elongation model for aza-BODIPY **1** in (S)-limonene (1.0 × 10^{-5} M) with a cooling rate of 0.5 K min^{-1}

Method	Nucleation		Elongation			
	K_a	N_n (T_e)	α_{SAT}	T_e/K	ΔH_e/kJ mol^{-1}	R^2
UV/Vis	0.00463	5–6	1.021	323 ± 0.6	−143 ± 1.9	0.996
CD	0.00017	17–19	1.078	310 ± 0.5	−149 ± 2.4	0.999

exhibited an average height of *ca.* 10 nm while their lengths were 0.5–3 μm. Such a helical morphology of dye **1** aggregates was further confirmed by TEM measurements (Fig. S8†). In AFM studies, both left-handed (*M*) and right-handed (*P*) helices were observed for the nanofibers of dye **1**. For an AFM image on a larger scale (Fig. S9a†), 39 (64%) left-handed and 22 (36%) right-handed helical aggregates were resolved, indicating the majority of left-handed (*M*) helices in (*S*)-limonene. Likewise, the helical fibers obtained in (*R*)-limonene exhibited a majority of 66% of right-handed (*P*) nanofibers (Fig. S9b†). In addition, an IR spectroscopy study on **Agg. II$_L$** (Fig. S10†) indicated that the intermolecular hydrogen bonding interactions between the chromophores played an important role in the aggregation process.

Based on all the results of the spectroscopic studies as well as the morphological studies, a mechanistic model for the self-assembly of dye **1** in chiral limonene was proposed (Fig. 3). Upon
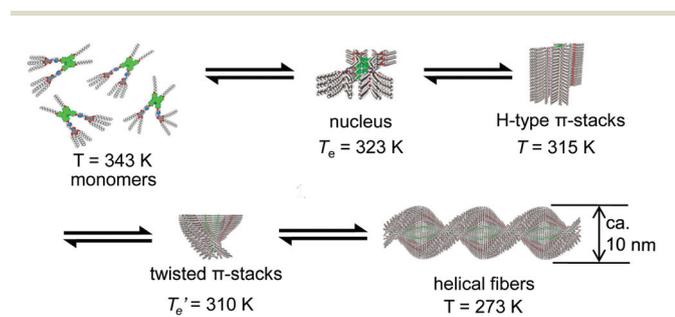
Fig. 3 Schematic assembly mechanism for the formation of helical fibrous aggregates **Agg. II$_L$** of dye **1** upon slow cooling from 343 K to 273 K in the chiral limonene solvent.

a slow decrease in temperature (*e.g.* 0.5 K min^{-1}), the monomers of dye **1** formed first short H-type, CD-inactive π-stacks through a cooperative process with T_e = 323 K as indicated by UV/Vis spectroscopy. Upon further cooling, a subsequent chiral transition may take place at 310 K under the induction of the chiral limonene solvent as indicated by CD spectroscopy, leading to the formation of small-sized twisted CD active π-stacks (chiral nuclei) which finally grow into helical fibrous stacks of dye **1** with the size in micrometers with supramolecular chirality. Accordingly, the CD monitored process (from CD inactive H-type π-stacks to CD active helical fibers) exhibited a much larger nucleus size N_n (see Table 1) and higher cooperativity (smaller K_a) than the assembly process monitored by UV/Vis spectroscopy.

Since **Agg. I$_L$** is kinetically unstable in the chiral limonene solvent, performing seeded living supramolecular polymerization (LSP) directly in these solvents was impractical. However, it has been well known that **Agg. I$_M$** can be kinetically trapped in MCH facilely by fast cooling and has been used for LSP in MCH successfully.[19] Thus, seeded supramolecular polymerization using the seeds of **Agg. II$_L$** in limonene and **Agg. I$_M$** in MCH was performed in the MCH/limonene solvent mixture (Fig. S11†). As shown by the kinetic curves, the transformation from **Agg. I$_M$** to **Agg. II$_L$** slows down gradually upon increasing the content of MCH from 10% to 70% in the solvent mixture while the ratio of [**Seed$_{Agg. III}$**]/[**Agg. I$_M$**] was kept as 1, as evidenced by t_{50} increasing quickly from 3 min to 54 min. When the content of MCH increased to 80%, no transformation was observed in the experimental period. Encouraged by these observations, multiple cyclic asymmetric LSP was carried out using **Agg. I$_M$** in MCH and **Agg. II$_L$** in (*S*)-limonene (Fig. 4 and
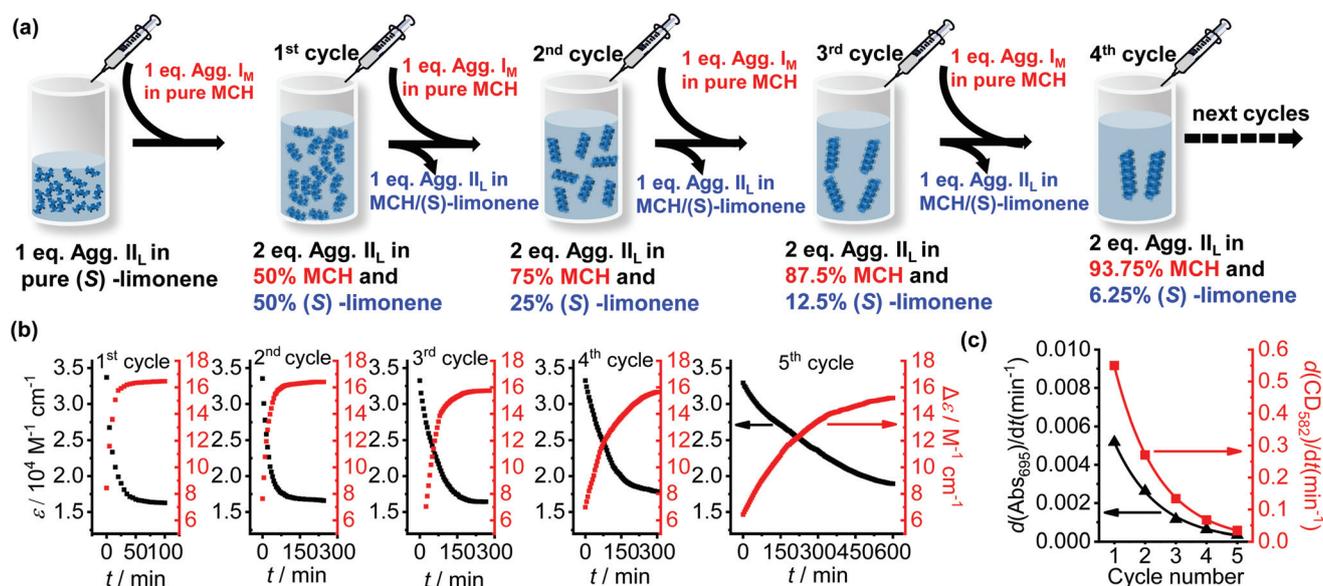
Fig. 4 (a) Schematic presentation of the experimental operation of multiple cyclic LSP at 283 K. (b) Time-dependent spectral changes for the LSP process in mixed MCH/limonene monitored by UV/Vis (black, 695 nm) and CD spectroscopy (red, 582 nm) ([**SeedAgg. II$_L$** in (*S*)-limonene] = [**Agg. I$_M$** in MCH] = 5.0 × 10^{-6} M). (c) Initial polymerization rates of (dAbs$_{695}$/dt) and (dCD$_{582}$/dt) for each cycle and the fitting curves by equations $y = (0.00518\ \text{min}^{-1})/2^{n-1}$ and $y = (0.54995\ \text{mdeg min}^{-1})/2^{n-1}$ for the data obtained by UV/Vis and CD spectroscopy, respectively, where n is the cycle number and the initial polymerization rates for the first cycles are 0.00518 min^{-1} (UV/Vis absorption) and 0.55 mdeg min^{-1} (CD).

3952 | *Org. Chem. Front.*, 2022, **9**, 3949–3955

This journal is © the Partner Organisations 2022

Fig. S12†). The experimental operation was the same as that applied for the LSP of **1** in MCH[19] except that the solvent for seeds was (*S*)-limonene. The seeded supramolecular polymerization was performed in multiple cycles and monitored by time-dependent UV/Vis absorption as well as CD spectroscopy (Fig. 4b). Based on these results, the initial polymerization rate of the nth cycle was evaluated with the equation $\nu^{nth} = \nu^{1st} \times 0.5^{(n-1)}$ for both methods (Fig. 4c) and the data points were found to be fitted well with the relationship, suggesting the chain-growth mechanism of the seeded supramolecular polymerization.

It is worth noting that with our method for LSP, the content of (*S*)-limonene in the solvent mixture was reduced by half for each cycle. Surprisingly, the transformation from **Agg. I$_M$** to supramolecular chiral aggregates can proceed in the fifth cycle, in which the content of the chiral solvent was about 3%. Furthermore, we observed that even in the seventh cycle with a chiral limonene content less than 1%, the transformation can still proceed (data not shown). This result can be explained by the chiral memory effect of the supramolecular chiral aggregates of dye **1**. Firstly, the molecular chirality of the limonene was transferred to the seeds of dye **1** aggregates, which further initiates the asymmetric supramolecular polymerization of dye **1**. Upon continuous dilution of the chiral component in the (*S*)-limonene/MCH solvent mixture, the supramolecular chirality of the aggregates was preserved since the process of transformation of chiral aggregates to achiral species is controlled by kinetics rather than thermodynamics.

After the multiple cyclic LSP process, when the chiral supramolecular aggregates were kept in solvents with a very low content of (*S*)-limonene, a slow racemization of the aggregates was observed. This phenomenon can be ascribed to the fact that the aggregates of dye **1** tend to transform to a thermo-dynamically more stable state. The racemization kinetics was monitored by CD spectroscopy at both 293 K and 283 K (Fig. 5). The half-decay time for the racemization process of **Agg. II$_L$** in the mixed solvent of MCH/limonene with a ratio of limonene of *ca.* 1% was about 11 days at 283 K, which was almost 2 times longer than that at 293 K (6 days).

Conclusions

In the chiral solvents (*S*)- and (*R*)-limonene, the aza-BODIPY **1** can assemble into metastable aggregates (**Agg. I$_L$**, kinetically trapping cannot be reached) as well as thermodynamically stable one-dimensional H-type helical aggregates (**Agg. II$_L$**) by cooperative π–π stacking and intermolecular hydrogen-bonding interactions, as demonstrated by the UV/Vis absorption and CD spectroscopic results as well as the morphological studies by AFM and TEM. By spectroscopic data analysis using the nucleation–elongation model, thermodynamic parameters including the critical elongation temperature and enthalpy changes were obtained, which indicated the enthalpy-driven assembly process of dye **1**. The AFM and CD spectroscopic studies showed that the handedness of the chiral supramolecular aggregates of **1** was found to be dependent on the chirality of the limonene solvents, *i.e.* enrichment of right-handed (*P*) helicity was observed in (*R*)-limonene, while left-handed (*M*) helicity was enriched in (*S*)-limonene. In addition, a mechanism for assembly of dye **1** from monomers to helical fibrous aggregates was proposed. Furthermore, a novel LSP strategy to obtain chiral supramolecular aggregates of achiral dye **1** in a nearly achiral environment using the chiral seeds of **1** in limonene and the kinetically trapped aggregates of **1** in MCH (**Agg. I$_M$**) was developed. With this LSP strategy, the chiral **Agg. II$_L$** can be obtained at a very low volume ratio of chiral limonene (less than 1%) in the MCH/limonene solvent mixture, which can be well explained by the chiral memory effect of **Agg. II$_L$** in the multiple polymerization cycles. In such a nearly achiral environment, the chirality of aggregates can last for quite a long period (about two weeks at 293 K) until the racemization process of the chiral aggregates was completed. Considering the functionality of the NIR absorption and emissive properties of aza-BODIPY dyes, the fibrous chiral nanoaggregates of dye **1** may offer new prospects for application in chiral sensing or chiroptical materials.

Conflicts of interest

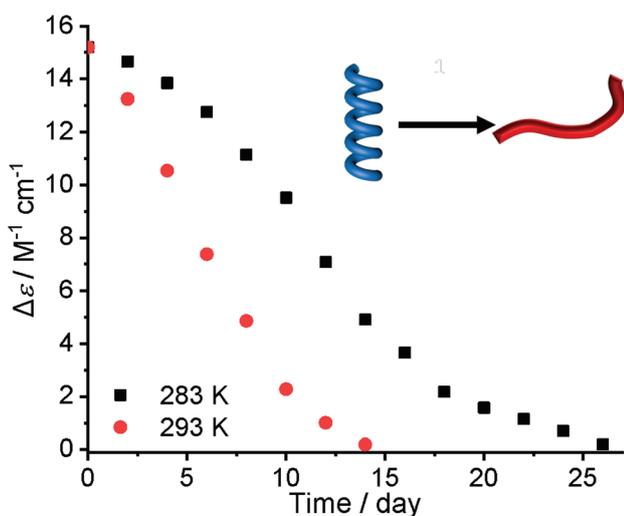There are no conflicts to declare.

Acknowledgements

Fig. 5 Time-dependent CD spectra of **Agg. II$_L$** in the MCH/limonene mixed solvent with a volume ratio of limonene of *ca.* 1% (after seven cycles LSP experiment, 5.0×10^{-6} M) at 283 K and 293 K (monitored at 582 nm).

This journal is © the Partner Organisations 2022

Org. Chem. Front., 2022, **9**, 3949–3955 | **3953**

Notes and references

1   (a) M. Liu, L. Zhang and T. Wang, Supramolecular Chirality in Self-Assembled Systems, *Chem. Rev.*, 2015, **115**, 7304–7397; (b) E. Yashima, N. Ousaka, D. Taura, K. Shimomura, T. Ikai and K. Maeda, Supramolecular Helical Systems: Helical Assemblies of Small Molecules, Foldamers, and Polymers with Chiral Amplification and Their Functions, *Chem. Rev.*, 2016, **116**, 13752–13990; (c) K. Ariga, T. Mori, T. Kitao and T. Uemura, Supramolecular Chiral Nanoarchitectonics, *Adv. Mater.*, 2020, **32**, 1905657; (d) S. Huang, H. Yu and Q. Li, Supramolecular Chirality Transfer toward Chiral Aggregation: Asymmetric Hierarchical Self-Assembly, *Adv. Sci.*, 2021, **8**, 2002132.

2   (a) A. Lohr and F. Würthner, Evolution of homochiral helical dye assemblies: Involvement of autocatalysis in the "Majority-Rules" effect, *Angew. Chem., Int. Ed.*, 2008, **47**, 1232–1236; (b) S. Yagai, Y. Nakano, S. Seki, A. Asano, T. Okubo, T. Isoshima, T. Karatsu, A. Kitamura and Y. Kikkawa, Supramolecularly Engineered Aggregation of a Dipolar Dye: Vesicular and Ribbonlike Architectures, *Angew. Chem., Int. Ed.*, 2010, **49**, 9990–9994; (c) I. De Cat, Z. Guo, S. J. George, E. W. Meijer, A. P. H. J. Schenning and S. De Feyter, Induction of Chirality in an Achiral Monolayer at the Liquid/Solid Interface by a Supramolecular Chiral Auxiliary, *J. Am. Chem. Soc.*, 2012, **134**, 3171–3177; (d) B. Mahlmeister, R. Renner, O. Anhalt, M. Stolte and F. Würthner, Axially chiral bay-tetraarylated perylene bisimide dyes as non-fullerene acceptors in organic solar cells, *J. Mater. Chem. C*, 2022, **10**, 2581–2591.

3   Z. Chen, Q. Wang, X. Wu, Z. Li and Y. B. Jiang, Optical chirality sensing using macrocycles, synthetic and supramolecular oligomers/polymers, and nanoparticle based sensors, *Chem. Soc. Rev.*, 2015, **44**, 4249–4263.

4   M. Weh, J. Ruhe, B. Herbert, A. M. Krause and F. Würthner, Deracemization of Carbohelicenes by a Chiral Perylene Bisimide Cyclophane Template Catalyst, *Angew. Chem., Int. Ed.*, 2021, **60**, 15323–15327.

5   G. Albano, G. Pescitelli and L. Di Bari, Chiroptical Properties in Thin Films of π-Conjugated Systems, *Chem. Rev.*, 2020, **120**, 10145–10243.

6   J. Liang, P. Guo, X. Qin, X. Gao, K. Ma, X. Zhu, X. Jin, W. Xu, L. Jiang and P. Duan, Hierarchically Chiral Lattice Self-Assembly Induced Circularly Polarized Luminescence, *ACS Nano*, 2020, **14**, 3190–3198.

7   C. Kulkarni, A. K. Mondal, T. K. Das, G. Grinbom, F. Tassinari, M. F. J. Mabesoone, E. W. Meijer and R. Naaman, Highly Efficient and Tunable Filtering of Electrons' Spin by Supramolecular Chirality of Nanofiber-Based Materials, *Adv. Mater.*, 2020, **32**, 1904965.

8   (a) P. A. Korevaar, S. J. George, A. J. Markvoort, M. M. J. Smulders, P. A. J. Hilbers, A. P. H. J. Schenning, T. F. A. De Greef and E. W. Meijer, Pathway complexity in supramolecular polymerization, *Nature*, 2012, **481**, 492–U103; (b) B. Vedhanarayanan, V. S. Nair, V. C. Nair and A. Ajayaghosh, Formation of Coaxial Nanocables with Amplified Supramolecular Chirality through an Interaction between Carbon Nanotubes and a Chiral p-Gelator, *Angew. Chem., Int. Ed.*, 2016, **55**, 10345–10349.

9   (a) S. Ghosh, X. Q. Li, V. Stepanenko and F. Würthner, Control of H- and J-Type π Stacking by Peripheral Alkyl Chains and Self-Sorting Phenomena in Perylene Bisimide Homo- and Heteroaggregates, *Chem. – Eur. J.*, 2008, **14**, 11343–11357; (b) T. E. Kaiser, V. Stepanenko and F. Würthner, Fluorescent J-Aggregates of Core-Substituted Perylene Bisimides: Studies on Structure-Property Relationship, Nucleation-Elongation Mechanism, and Sergeants-and-Soldiers Principle, *J. Am. Chem. Soc.*, 2009, **131**, 6719–6732; (c) M. Wehner, M. I. S. Rohr, V. Stepanenko and F. Würthner, Control of self-assembly pathways toward conglomerate and racemic supramolecular polymers, *Nat. Commun.*, 2020, **11**, 5460.

10   W. Zhang, W. Jin, T. Fukushima, T. Mori and T. Aida, Helix Sense-Selective Supramolecular Polymerization Seeded by a One-Handed Helical Polymeric Assembly, *J. Am. Chem. Soc.*, 2015, **137**, 13792–13795.

11   E. Yashima, N. Ousaka, D. Taura, K. Shimomura, T. Ikai and K. Maeda, Supramolecular Helical Systems: Helical Assemblies of Small Molecules, Foldamers, and Polymers with Chiral Amplification and Their Functions, *Chem. Rev.*, 2016, **116**, 13752–13990.

12   (a) M. Wolffs, J. L. J. Van Velthoven, X. Lou, R. A. A. Bovee, M. Pouderoijen, J. L. J. Van Dongen, A. P. H. J. Schenning and E. W. Meijer, Influence of the Solvent and the Enantiomeric Purity on the Transition between Different Supramolecular Polymers, *Chem. – Eur. J.*, 2012, **18**, 15057–15064; (b) M. L. Śleczkowski, M. F. J. Mabesoone, P. Śleczkowski, A. R. A. Palmans and E. W. Meijer, Competition between chiral solvents and chiral monomers in the helical bias of supramolecular polymers, *Nat. Chem.*, 2021, **13**, 200–207.

13   P. Qin, Z. Wu, P. Li, D. Niu, M. Liu and M. Yin, Triple-Modulated Chiral Inversion of Co-Assembly System Based on Alanine Amphiphile and Cyanostilbene Derivative, *ACS Appl. Mater. Interfaces*, 2021, **13**, 18047–18055.

14   J. M. Ribó, J. Crusats, F. Sagués, J. Claret and R. Rubires, Chiral sign induction by vortices during the formation of mesophases in stirred solutions, *Science*, 2001, **292**, 2063–2066.

15   S. Du, X. Zhu, L. Zhang and M. Liu, Switchable Circularly Polarized Luminescence in Supramolecular Gels through Photomodulated FRET, *ACS Appl. Mater. Interfaces*, 2021, **13**, 15501–15508.

16   R. Purrello, Supramolecular chemistry - Lasting chiral memory, *Nat. Mater.*, 2003, **2**, 216–217.

17   S. J. George, Ž. Tomović, M. M. J. Smulders, T. F. A. de Greef, P. E. L. G. Leclère, E. W. Meijer and A. P. H. J. Schenning, Helicity Induction and Amplification in an Oligo(p-phenylenevinylene) Assembly through Hydrogen-Bonded Chiral Acids, *Angew. Chem., Int. Ed.*, 2007, **46**, 8206–8211.

18 V. Stepanenko, X. Q. Li, J. Gershberg and F. Würthner, Evidence for Kinetic Nucleation in Helical Nanofiber Formation Directed by Chiral Solvent for a Perylene Bisimide Organogelator, *Chem. – Eur. J.*, 2013, **19**, 4176–4183.

19 H. Wang, Y. Zhang, Y. Chen, H. Pan, X. Ren and Z. Chen, Living Supramolecular Polymerization of an Aza-BODIPY Dye Controlled by a Hydrogen-Bond-Accepting Triazole Unit Introduced by Click Chemistry, *Angew. Chem., Int. Ed.*, 2020, **59**, 5185–5192.

20 (*a*) P. Jonkheijm, P. van der Schoot, A. P. H. J. Schenning and E. W. Meijer, Probing the solvent-assisted nucleation pathway in chemical self-assembly, *Science*, 2006, **313**, 80–83; (*b*) M. M. J. Smulders, M. M. L. Nieuwenhuizen,

T. F. A. de Greef, P. van der Schoot, A. P. H. J. Schenning and E. W. Meijer, How to distinguish isodesmic from cooperative supramolecular polymerisation, *Chem. – Eur. J.*, 2010, **16**, 362–367; (*c*) Y. Liu, Y. Zhang, F. Fennel, W. Wagner, F. Würthner, Y. Chen and Z. Chen, Coupled Cooperative Supramolecular Polymerization: A New Model Applied to the Competing Aggregation Pathways of an Amphiphilic aza–BODIPY Dye into Spherical and Rod–Like Aggregates, *Chem. – Eur. J.*, 2018, **24**, 16388–16394.

21 P. Jonkheijm, P. van der Schoot, A. P. H. J. Schenning and E. W. Meijer, Probing the solvent-assisted nucleation pathway in chemical self-assembly, *Science*, 2006, **313**, 80–83.

This journal is © the Partner Organisations 2022

Org. Chem. Front., 2022, **9**, 3949–3955 | **3955**